# Application of the wavelet transform to nanoscale thermal transport

Christopher H. Baker,* Donald A. Jordan, and Pamela M. Norris†
*Department of Mechanical and Aerospace Engineering, University of Virginia, Charlottesville, Virginia 22904, USA*
(Received 16 May 2012; revised manuscript received 7 September 2012; published 20 September 2012)

The continuous wavelet transform is employed to analyze the dynamics and time-dependent energy distribution of phonon wave-packet propagation and scattering in molecular dynamics simulations. The equations of the one-dimensional continuous wavelet transform are presented and then discretized for implementation. Practical aspects and limitations of the transform are discussed, with attention to its application in the analysis of molecular dynamics simulations. The transform is demonstrated using three examples that are relevant to nanoscale thermal transport. First, a system of wave packets that interfere in both the spatial and Fourier domains are separated by the wavelet transform, allowing the measurement of each packet's contribution to the system energy. Second, the wavelet transform is applied to a multiple wave-packet simulation of a silicon, heavy-silicon interface. The wavelet-based calculation of mode-dependent transmission is validated through comparison to literature results and theoretical predictions. Third, the dynamic scattering of a large amplitude wave packet is studied using the wavelet transform. The transform reveals a transition in the structure of the energy distribution. Unlike current techniques, the wavelet transform can be used to determine how the energy of a simulated system is distributed in time, in space, and among wave numbers, simultaneously. The ability to resolve phonon motion and energy from a vibrating ensemble of atoms in a molecular dynamics simulation makes the wavelet transform a promising technique for probing the physical mechanisms of nanoscale thermal transport.

DOI: 10.1103/PhysRevB.86.104306 PACS number(s): 63.22.−m, 02.70.Ns, 44.05.+e

## I. INTRODUCTION

Modern fabrication techniques have made possible the design and synthesis of technological devices at the nanoscale. Recently, transistor elements in consumer microprocessors reached the characteristic size of 22 nm. Furthermore, current strategies for enhancing the thermoelectric figure of merit[1–5] and efficiencies of solar cells[6] are based on quantum-well structures resulting from the careful design of materials at the nanoscale. The performance of these devices is intimately related to their ability to dissipate thermal energy, for microprocessors and solar cells, or inhibit thermal transport, for thermoelectrics. Optimization of the thermal properties of these devices will depend on precise control of thermal energy flow through the nanoscale heterogeneous features characteristic of these technologies.

The thermal transport across a heterogeneous structure, such as an interface, arises from two contributions: each material's intrinsic properties and the auxiliary effects of the interface's presence. The intrinsic properties of phonon dispersion, density of states, and phonon-phonon scattering times determine the thermal conductivity of the constituent materials.[7] The dispersion and density of states have been utilized in the acoustic mismatch model[8] and diffuse mismatch model,[9] along with derivative models, to predict thermal boundary conductance. The intrinsic properties can be computed analytically for moderate temperatures using harmonic or anharmonic lattice dynamics,[10] along with scattering approximations of various complexities.[11] The second contributor is the influence of the interface's presence on the local phonon population, which is less fully understood. Scattering of phonons by the interface may create coherent effects,[12] defects due to a mismatch in lattice parameters are themselves a source of scattering, and the occupied density of states is altered in the vicinity of the interface.[13] These effects are difficult, if not impossible, to experimentally isolate, leading to simulation as the preferred method of studying the mechanisms of thermal boundary conductance.

A crucial aspect of thermal boundary conductance is the mode-dependent phonon transmission factor across an interface. This information can be obtained analytically using nonequilibrium Green's functions[14,15] and scattering boundary methods[16,17] or through simulation using the wave-packet method.[18] In the wave-packet method, a single localized phonon is constructed by enveloping a normal mode of the crystal in a Gaussian distribution. This wave-packet propagates toward an interface, then scatters into a transmitted and reflected portion according to classical wave theory. In contrast to the analytical methods, the wave-packet method captures the transient and localized scattering of the phonon by the interface. This property makes the technique suited to studying the effects of interface structure on phonon transmission. The phonon transmission as a function of wave number, polarization, and phonon branch provides a key element of thermal boundary conductance modeling.

Wave-packet simulations have been used to study epitaxial semiconductor interfaces,[18] textured semiconductor interfaces,[19] silicon-to-carbon nanotube interfaces,[20] self-assembled monolayer interfaces,[21] thermal rectification,[22] and thin films.[23] Research in this area has focused on the simulation of one incident wave packet at a time (although simulations with multiple wave packets are possible[24]), in a zero Kelvin system, where the transmission is determined by summing the kinetic and potential energies on either side of the interface after the wave-packet scattering process has occurred. A limitation of this approach, or any other simulation technique, is that it is unable to capture the mechanisms of the energy transfer during the time the packet interacts with the interface due to the nonequilibrium, non-steady-state, and especially, localized nature of the process. Understanding the mechanisms by which the features of an interface affect

 

the phonon transport will enable the prediction of thermal boundary conductance and subsequent design of interfaces for device applications.

In this work, the wavelet transform is presented as a solution for overcoming this challenge and other challenges related to localized phonon physics. The wavelet transform is a mathematical tool developed within the last few decades that decomposes a signal by both location and wave number. Thus, it might be thought of as a compromise between representations of a signal in the spatial and Fourier domains. Whereas the Fourier transform uses a complex exponential basis, the wavelet basis function is localized in both space and wave number. In the context of nanoscale thermal transport, the Fourier transform is crucial to the techniques of normal mode decomposition[25,26] and density of states calculation,[13,27] not to mention the concept of reciprocal space.[28] Each of these tools gives vibrational information from a series of space or time-dependent atomic properties. Nevertheless, they can not tell where or when those vibrations occurred in the untransformed series.[29] Not only does the wavelet transform provide vibrational information, it also retains information on where or when those vibrations occurred. This capability allows more in-depth study of spatially constrained vibrational processes, such as phonon-phonon scattering and interface scattering. Although the coordinates of location and wave number are used throughout this work, time and frequency are completely analogous and the same wavelet transform equations apply.

Farge presents a history of the development of the wavelet transform in her review on the topic.[30] Following its derivation, the wavelet transform found applications in such diverse fields as geophysics,[31] signal processing,[32] data compression,[33] turbulence,[30] and meteorology.[34] To the authors' knowledge, the wavelet transform has only been used once thus far in the context of molecular dynamics simulation and nanoscale thermal transport. In a study by Shiomi and Maruyama, the wavelet transform was used to track the phonon spectral peak position and velocity following an ultrafast heating event in a simulated carbon nanotube.[35] The lack of representation in the literature does not reflect the potential of this technique for studying a variety of phonon scattering problems. This work aims to demonstrate this application in order that the wavelet transform may be more widely used in future investigations of phonon physics in molecular dynamics simulation.

In Sec. II, the equations describing the continuous wavelet transform are presented. Their adaptation for a discrete system is then provided. Whereas the Fourier transform has but one basis, many possibilities exist for the wavelet transform. In this development, the Morlet wavelet (Fig. 1) is chosen because of its simplicity and resemblance to a wave packet. The equations are developed with the goal of clarity and ease of implementation without mathematical derivation as this has been presented elsewhere[36] and would detract from the aforementioned goals of this paper. The method of applying the wavelet transform to analyze the spatiovibrational distribution of energy in a molecular dynamics simulation will then be presented. In Sec. III, the time, location, and wave-number resolved distribution of energy afforded by the wavelet transform is quantitatively demonstrated in the context of molecular dynamics simulation and nanoscale thermal transport. Three wave-packet systems will be used for this purpose. First, the transform is used as a filter to determine the individual contributions of interfering packets to the system energy. Second, the transform is applied to a wave-packet interface study in molecular dynamics simulation with multiple extraneous packets present. Third, the anharmonic scattering of a high-amplitude wave packet is studied using the wavelet transform.

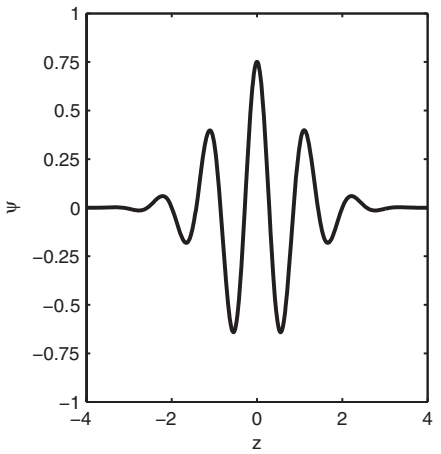


FIG. 1. The real part of the Morlet wavelet given by Eq. (12). The parameter $k_\psi$ is 5.5 and corresponds to the number of oscillations spanning the wavelet.

## II. METHODS

### A. Continuous wavelet transform

The wavelet transform uses wavelets as the analyzing function just as the Fourier transform uses complex exponentials. In order for a function to be considered a wavelet, it must satisfy two primary conditions.[30] The first, termed the admissibility condition, states that the function must have a mean of zero. The second is that the function must be localized in both space and wave number. Taking the complex exponential basis of the Fourier transform, we immediately see that it can not be considered a wavelet since, although it satisfies the admissibility condition, it is not localized in space. There are a multitude of wavelets that are used in the wavelet transform. The presentation of the transform will at first remain general with respect to both the functional form of the wavelet and the specific application to molecular dynamics simulation. The equations follow the development of the transform presented in Kaiser's book.[36]

The wavelet transform is obtained through application of a set of wavelet filters to a signal. Each filter is obtained from an original wavelet by translating it and dilating it.[30] The original wavelet is called the mother wavelet and its altered forms are called daughter wavelets. The equation for the daughter wavelets is[36]

$$\psi_{s,\delta}(z) = |s|^{-1/2}\psi\left(\frac{z-\delta}{s}\right), \tag{1}$$

where $z$ is a spatial coordinate, $\psi(z)$ is the mother wavelet, $s$ is the scale factor that controls dilation, and $\delta$ is the displacement of the wavelet with respect to the signal. The scale factor

can be interpreted as a form of the wavelength and we shall see later that it is indeed proportional to the wavelength and inversely proportional to the wave number for the Morlet wavelet (Fig. 1). The leading power of $s$ is an arbitrary choice as indicated by Kaiser.[36] A power of negative one-half is chosen to make the energies defined by the $L^2$ norm of each daughter wavelet the same as that of the mother wavelet. In the remainder of this work, "energy" shall refer to this signal-processing-based definition, which is distinct from the physical quantity of energy, although they are related. When the physical definition is intended, it will be specified as kinetic or potential energy.

Once the daughter wavelets are defined, the transform is accomplished by a correlation integral with the signal

$$\tilde{f}(s,\delta) = \int_{-\infty}^{\infty} \psi^*_{s,\delta}(z) f(z) dz, \tag{2}$$

where the tilde indicates the wavelet coefficient function, the asterisk denotes the complex conjugate, and $f(z)$ is a one-dimensional signal. The equations can be adjusted to include multiple spatial dimensions along with time and even rotations, although this is outside the scope of the current work.[30]

In order for the transform to be useful, the inverse transform must reproduce the original signal. The inverse transform, called the reconstruction formula, is given as[36]

$$f(z) = \frac{1}{C} \int_{-\infty}^{\infty} \int_{-\infty}^{\infty} |s|^{-2} \psi_{s,\delta}(z) \tilde{f}(s,\delta) ds\, d\delta, \tag{3}$$

where $C$ is the admissibility constant. The requirement that the analyzing wavelet have a mean of zero is equivalent to the requirement that $C$ be a nonzero, finite number, given by

$$C = \int_{-\infty}^{\infty} \frac{|\hat{\psi}(\xi)|^2}{|\xi|} d\xi < \infty, \tag{4}$$

where $\hat{\psi}$ is the Fourier transform of the mother wavelet. The variable $\xi$ is used instead of $k$ to emphasize the nondimensional nature of the mother wavelet. There are three variations of the Fourier transform and its inverse that all differ by a factor of $2\pi$.[36] The form of the Fourier transform used in this work is explicitly defined for an arbitrary signal $h(z)$ as

$$\hat{h}(k) = \int_{-\infty}^{\infty} h(z) \exp(-2\pi i k z) dz. \tag{5}$$

This variation of the Fourier transform converts the signal $h$ to a nonradial wave-number domain. The inverse Fourier transform is generated by switching $h(z)$ and $\hat{h}(z)$ and changing the sign of the exponent. In this way, $k$ has the physical interpretation of inverse length. By the Plancherel theorem, also known as Rayleigh's theorem,[37,38] the energy of the signal is conserved regardless of the domain:

$$\begin{aligned} \|f\|^2 &= \int_{-\infty}^{\infty} |f(z)|^2 dz = \int_{-\infty}^{\infty} |\hat{f}(k)|^2 dk \\ &= \frac{1}{C} \int_{-\infty}^{\infty} \int_{-\infty}^{\infty} |s|^{-2} |\tilde{f}(s,\delta)|^2 ds\, d\delta. \end{aligned} \tag{6}$$

As demonstrated by the above equations, the wavelet transform is a scientific tool for the study of complicated functions of space (time) where potential phenomena of interest depend on both location (time) and wave number (frequency). In the context of nanoscale thermal transport, phonons represent just such a phenomenon: they are the quantized normal modes of vibration of a crystal, yet can also be considered quasiparticles due to wave-particle duality. In order to use the wavelet transform to examine individual phonons, one must measure the atomic displacements caused by the phonons, an impossible experimental task. Yet, the computational tool of molecular dynamics simulation provides just such a vehicle for investigation of phonon physics using the wavelet transform. In order to harness the wavelet transform for this task, the equations presented above must be discretized to a form that can be implemented in computer code.

### B. Discretized equations

Although discretized implementations of the continuous wavelet transform have been presented before,[34,39] this presentation is unique in that it follows directly from the continuous equations and synthesizes certain aspects of the implementations from the previous works. The resulting transform conserves the signal energy and is completely reversible. As an overview, the set of daughter wavelets are calculated using dimensional coordinates (as opposed to nondimensional), in accordance with the work of Kaiser[36] and Torrence and Compo.[34] This provides the flexibility to take the wavelet transform of a system with nonconstant sample spacing, e.g., a heterogeneous crystalline system with more than one lattice constant where some atomic property is sampled at each monolayer. Such a sampling is impossible for real systems, but easily obtained in molecular dynamics simulations. This capability precludes the use of the convolution theorem and Fourier transforms to calculate the wavelet transform more rapidly, and so this method is not presented here.[34,39]

In going from the continuous to the discrete equations, the spatial coordinate $z$ becomes a vector of size $N$ ranging from $z_1$ to $z_N$. The integrations that span all of space are changed to summations over a finite interval. The wavelet transform [Eq. (2)] becomes

$$\tilde{f}(s,\delta) = \sum_{z=z_1}^{z_N} \psi^*_{s,\delta}(z) f(z) \Delta z, \tag{7}$$

where $\Delta z$ is the sample spacing of $z$. In general, the sample spacing need not be constant, as is the case for two different crystalline materials joined at an interface, and so $\Delta z$ is kept inside the summation. Technically, the values of $\delta$ need not fall on the locations of $z$, nor even have the same resolution as $z$. At times, it is necessary to make $\delta$ more coarse than $z$ in order to make the transform computationally tractable.[34] This flexibility in the selection of the $\delta$ coordinates is lost when using the Fourier transform with the convolution theorem to carry out the wavelet transform as is recommended in some other works.[34,39] The reconstruction [Eq. (3)] and energy [Eq. (6)] formulas become

$$f(z) = \frac{2}{C} \sum_{\delta} \sum_{s} |s|^{-2} \psi_{s,\delta}(z) \tilde{f}(s,\delta) \Delta s\, \Delta\delta \tag{8}$$

and

$$||f||^2 = \frac{2}{C}\sum_{\delta}\sum_{s}|s|^{-2}|\tilde{f}(s,\delta)|^2\Delta s\Delta\delta. \tag{9}$$

Here, the summation is over only the positive scales and the even symmetry of $\tilde{f}$ with respect to the scale results in the coefficient of 2. This is procedurally similar to typical applications of the Fourier transform, where negative frequencies are disregarded. Typically, the signal to be analyzed is real and thus the real part of Eq. (8) is taken to reproduce the signal. In practice, trapezoidal numerical integration, or a more sophisticated numerical method, should be used to minimize error.

A key advantage of the wavelet transform is that it enables the calculation of energy in a window of $z$-$s$ space. The kinetic theory of phonons models phonons as point particles with a definite position and wave vector. By calculating the energy within a window of $z$-$s$ space, the wavelet transform is used to find the energy associated with an ensemble of phonons within a certain spatial and wave-number range. To accomplish this, the bounds of the summations in Eqs. (8) and (9) are adjusted to include the desired area of the wavelet domain. For visualization purposes, it is convenient to define the wavelet energy density $\rho$ as

$$\rho \equiv \frac{2}{C}|s|^{-2}|\tilde{f}|^2. \tag{10}$$

In this way, the relative magnitudes of energies at different locations may be estimated in plots of the wavelet energy density. The equation of the admissibility constant has been appropriately altered:

$$C = \Delta\xi\sum_{\xi=\xi_2}^{\xi_N}\frac{|\hat{\psi}(\xi)|^2}{|\xi|}. \tag{11}$$

Conversion of Eqs. (4) to (11) and the resulting numerical integration requires that the $\xi_1 = 0$ point be removed to avoid division by zero, even though the integrand approaches zero as $\xi$ approaches zero.

### C. Morlet wavelet and implementation

Now that the continuous and discretized versions of the equations have been laid out, the practical aspects concerning the implementation of the technique are presented. The particulars follow the work of Jordan *et al.*[39] with a key difference being how the scales to be analyzed are determined, being motivated by the significance of reciprocal space to phonon transport. Although there are an infinite number of wavelets that satisfy the admissibility and localization requirements, the Morlet wavelet[31] as depicted in Fig. 1 is often used[34,35,39] because of its simple form and interpretation as a plain wave in a Gaussian envelope function (the same form as a wave packet, discussed in Sec. III):

$$\psi(z) = \pi^{-1/4}\exp(ik_\psi z)\exp(-1/2z^2), \tag{12}$$

where $k_\psi$ is the peak angular wave number. The factor of $\pi^{-1/4}$ normalizes the wavelet to have unit energy. As Farge notes, the mean value of the Morlet wavelet is not identically zero for arbitrary $k_\psi$.[30] Taking the half-width of the wavelet as 3, for values of $k_\psi$ greater than 4, the deviation from a mean of zero is less than one part in one thousand. For $k_\psi$ equal to 5.5, as used in this study, the error is on the order of 1 part in 10 000. This error is less than what can be expected from the inherent uncertainty introduced to the system by the transform, and thus it can be ignored. The choice of $k_\psi$ determines the tradeoff between spatial and wave-number resolution, although this aspect of the transform is not explored further here.[40]

With the mother wavelet defined, the daughter wavelets are found by substitution according to Eq. (1):

$$\psi_{s,\delta}(z) = \pi^{-1/4}|s|^{-1/2}\exp\left(ik_\psi\left[\frac{z-\delta}{s}\right]\right) \times \exp\left(-\frac{1}{2}\left[\frac{z-\delta}{s}\right]^2\right). \tag{13}$$

The Fourier transform of the mother wavelet, for use in Eq. (11), is also found to be

$$\hat{\psi}(\xi) = \sqrt{2}\pi^{1/4}\exp\left[-\tfrac{1}{2}(2\pi\xi - k_\psi)^2\right]. \tag{14}$$

The next task is to determine the restrictions placed on $s$. The lower limit of $s$ is found through aliasing considerations.[39] Applying Eqs. (5) to (13) results in the scale-dependent representation in Fourier space

$$\hat{\psi}_s(k) = \sqrt{2}\pi^{1/4}|s|^{1/2}\exp\left[-\tfrac{1}{2}(2\pi sk - k_\psi)^2\right]. \tag{15}$$

Note that the peak wave number is inversely proportional to $s$. Because the signal is sampled with some finite interval, the Fourier transform of the daughter wavelet with the smallest scale must decay to an acceptably small value by the Nyquist wave number in order to avoid aliasing (Fig. 2). This is represented mathematically by

$$\eta = \frac{\hat{\psi}_s(k_N)}{\hat{\psi}_s(k_p)}, \tag{16}$$

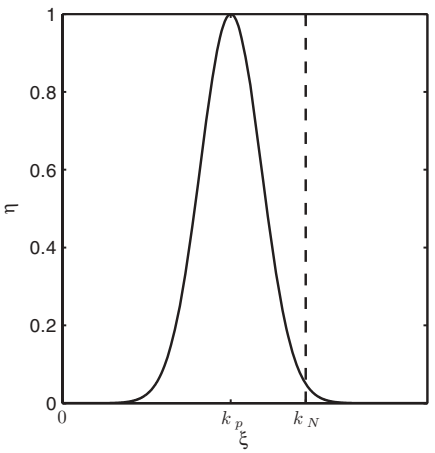


FIG. 2. Representation of a normalized, high-wave-number (small-scale) wavelet in the Fourier domain. The scale of the wavelet defines a peak wave number associated with the wavelet. The localized nature of the wavelet results in broadening of the spectral peak. The smallest scale must be chosen such that the peak decays to an acceptably small value by the Nyquist wave number. Here, that value is $\eta = 0.05$.

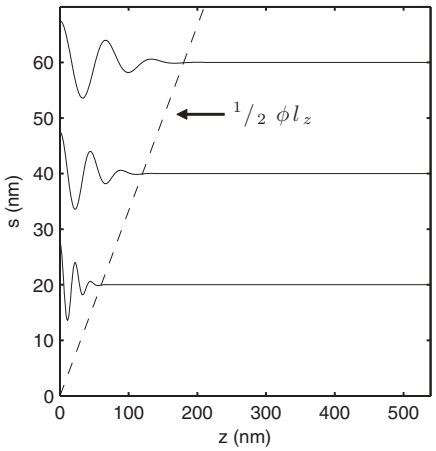


FIG. 3. Determination of edge effects. Depicted is the ingress of edge effects into the domain as a function of the scale. The form of the Morlet wavelet gives a linear relationship between the wavelet scale and the size of the edge effects, denoted by the dashed line. The amplitudes of the plotted wavelets are for visualization purposes.

where $\eta$ is the fractional decay, $k_N$ is the Nyquist wave number equal to $\frac{1}{2\Delta z}$, and $k_p$ is the peak wave number of $\frac{k_\psi}{2\pi s}$. For a nonconstant sample spacing, the largest value of the vector $\Delta z$ should be taken as the most conservative condition for avoiding aliasing. Solving for $s$ gives

$$s_1 = \frac{\Delta z}{\pi}(k_\psi + \sqrt{-2\ln(\eta)}). \tag{17}$$

The condition for the maximum scale factor is determined by edge effects. Just as with the Fourier transform, the finite length of the signal causes artifacts. For the wavelet transform, the artifacts are localized near the edges because of the finite width of its basis function, the wavelet. The artifacts extend further into the domain for larger scales. Therefore, there is a fundamental tradeoff between measuring phenomena at larger scales (lower wave numbers) and having fewer of the wavelet coefficients at those scales meaningful.[39] The fraction of the domain affected by these artifacts at the largest scale is defined as $\phi$. The encroachment of the effects into the domain is approximated by the half-width of the wavelet at that scale (Fig. 3). Noticing that $s$ is the standard deviation of the Gaussian envelope, the form of the Morlet wavelet provides a simple expression for the wavelet width. Letting the half-width equal $3s$ results in the maximum scale

$$s_M = \frac{\phi l_z}{6}, \tag{18}$$

where $l_z$ is the domain length. For truly periodic signals, edge artifacts can be avoided altogether. In this case, each of the analyzing wavelets is computed for a periodic space through the following adjustment to the wavelet's spatial coordinate:

$$z' = \begin{cases} z + l_z & \text{if} \quad z < \delta - \frac{l_z}{2}, \\ z & \text{if} \quad \delta - \frac{l_z}{2} \leqslant z \leqslant \delta + \frac{l_z}{2}, \\ z - l_z & \text{if} \quad z > \delta + \frac{l_z}{2}. \end{cases} \tag{19}$$

In the case that the sample spacing is uniform, $l_z$ is equal to $N\Delta z$. This periodicity condition causes the wavelets to wrap around the domain, mimicking the behavior of a system with periodic boundary conditions.

The previous three sections have laid out the methodology of performing the wavelet transform and the accompanying considerations. This presentation is equally applicable to any field, although particular reference has been made to nanoscale thermal transport in general and molecular dynamics simulation specifically. The next section reinforces how the above equations may be used to post-process molecular dynamics results in order to calculate the energy present at a specific location within the crystal and for a specific mode (wave number).

### D. Application to molecular dynamics simulation

The periodic arrangement of atoms in a crystalline solid gives rise to thermal energy transport mediated by phonons, the quantized normal modes of vibration of the lattice. The normal modes, by definition, have a well-defined wave number and frequency. Additionally, phonons can be treated as point particles, i.e., location is a property of the phonon. As shown in Secs. II A, II B, and II C, the wavelet transform can be used to study the behavior of systems where the dynamics depend on both location and wave number. The roles of location and wave number in thermal transport are most clearly displayed in wave-packet simulations, where one or more phonon modes are carefully constructed within the system. Although molecular dynamics simulation is a classical technique and can not inherently represent a quantized phonon, a wave packet might be thought of as a group of phonons, all with the same location, wave number, and branch. Like the Fourier transform, the wavelet transform is merely a mathematical tool and there are some post-processing steps required to convert the output of a molecular dynamics simulation into a signal on which the wavelet transform can operate. This section discusses these steps, as well as how the equations of Sec. II C are applicable.

The one-dimensional wavelet transform is applicable to molecular dynamics simulations for which material properties or a phenomenon of interest vary with only one dimension. Examples of such simulations include transport in homogeneous crystals, transport normal to a material interface, or cross-plane transport in a superlattice. The fluctuation to be analyzed, $f$, is generated by averaging some property of the atomic planes perpendicular to this direction. Planar displacement and velocity are examples of planar properties, the variations in space and wave number of which may be of interest. The displacement of a monolayer is related to the superposition of phonon modes present in the system.[10] In this case, the mean displacement of a monolayer can be taken as the signal to be analyzed. These displacements are defined with respect to the polarization vector of the phonon branch to be studied. The displacement $u$ of a primitive cell $l$ from a lattice dynamics perspective is[10]

$$u_l = \sum_j \vec{u}(lj) \cdot \epsilon(j), \tag{20}$$

where $\vec{u}(lj)$ is the displacement of the $j$th atom of the $l$th primitive cell and $\epsilon(j)$ is the polarization vector of the $j$th atom for a particular branch in the crystallographic direction collinear

with $z$. For the one-dimensional transform, the displacements of primitive cells that share a $z$ coordinate are averaged to obtain the spatially varying signal. For the [0 0 1] direction of cubic crystals, this procedure is rather straightforward. If analyzing phonon behavior in an arbitrary direction, it is recommended that the crystal coordinates be transformed such that the direction of interest coincides with the $z$ axis before the simulation is conducted. At low temperatures, the lack of atomic migration makes the predefinition of the monolayers possible. At higher temperatures, where atoms might migrate, the primitive cell and basis identity of each atom must be determined during the simulation or in post-processing.

Once the signal is generated, the limits of $s$ are found according to Eqs. (17) and (18). The smallest scale is limited by the sample spacing of $z$. For an ideal crystal, $\Delta z$ is a scalar found by projection of the appropriate primitive lattice vector onto the coordinate system of the conventional cell. Thus, $\Delta z$ can also be found from the crystal lattice and lattice constant, e.g., $\Delta z$ is equal to the lattice constant for simple cubic or half of the lattice constant for face-centered cubic crystals. A two-material system joined by an interface will exhibit differing values of $\Delta z$ far from the interface and a gradation of $\Delta z$ at the interface where strain develops due to the lattice mismatch. In this case, using the largest value of $\Delta z$ will ensure no aliasing in the signal analysis.

The largest scale is determined by the length of the simulation domain. For nonperiodic boundary conditions in the $z$ direction, the upper limit of $s$ is dictated by Eq. (18). Conversely, a simulation with periodic boundary conditions in the $z$ direction may take advantage of Eq. (19) to remove edge effects associated with large scales (small wave numbers). In this case, $\phi$ is set to 1.0 to obtain the smallest wave number that may be analyzed.

Once the minimum and maximum scales are found, these values are converted to the maximum and minimum wave numbers, respectively, by inversion: $k = \frac{k_\psi}{2\pi s}$. The analyzable wave numbers are generated within this range. Representation of the signal in $z$-$k$ is conducive to visualization, however, all analysis must be undertaken in the $z$-$s$ domain.

## III. APPLICATIONS

Wave-packet simulations best exemplify the role of localized vibrations, i.e., phonons, in nanoscale thermal transport. To this end, they also provide a simple and intuitive, yet physically relevant demonstration of how the wavelet transform can be used to study the location and wave-number-dependent distribution of energy as the wave packets propagate and scatter. Wave packets are constructed by specifying a coordinate-dependent displacement in the ideal (zero Kelvin) crystal according to the equation[18]

$$u(z) = A\epsilon(k_p)\exp\{2\pi i[k_p(z - z_p) - \omega_p t]\} \times \exp[-(z - z_p)^2/\zeta^2], \quad (21)$$

where $u$ is the displacement, $A$ is the amplitude, $\epsilon$ is the polarization vector, $k_p$ is the peak wave number, $z_p$ is the peak location of the wave packet, $\omega_p$ is the frequency corresponding to $k_p$, $t$ is time, and $\zeta$ is proportional to the width of the packet. In wave-packet simulations, $A$ is typically set to less than 1% of the lattice constant to avoid anharmonic effects. The small displacements allow a harmonic approximation and $\epsilon$ and $\omega_p$ can be computed using harmonic lattice dynamics for the wave number $k_p$.[10] Because the wave-packet representation of the phonon is localized in space, its Fourier spectrum is broadened about the peak value $k_p$. Setting $\zeta$ to a sufficiently large value causes the spectral peak to narrow. Preparing the wave packet for a molecular dynamics simulation also requires specification of the atomic velocities, which are found by differentiating Eq. (21) with respect to time. It is convenient to set time equal to zero for the displacements that define the start of the simulation.

### A. Filtering

Often times, a system under investigation contains some phenomenon that is obscured by extraneous information or noise. The act of filtering uses some characteristic of the desired phenomenon to differentiate it from the rest. For instance, the Fourier transform has seen unparalleled success in using frequency to distinguish a particular signal from a noisy whole. Methods of spectral analysis in molecular dynamics, such as normal mode decomposition,[25,26] depend on the properties of the Fourier transform. Here, the wavelet transform will be used in a similar sense, using not only frequency (wave number), but also location to determine the individual energies of superposed signals.

Three wave packets were constructed according to Eq. (21) with parameters defined in Table I and superimposed [Fig. 4(a)]. Because the wave-packet properties in this example are designated beforehand, the accuracy with which a given technique measures a certain property can be directly quantified. Calculation of individual wave-packet properties, such as energy, requires isolation of each packet and then application of the appropriate form of Eq. (6), which can involve the original spatial domain, the Fourier wave-number domain, or the wavelet domain. In the spatial domain, there is too much overlap in packets 1 and 2 to reasonably differentiate them [Fig. 4(a)]. The Fourier transform is able to separate packets 1 and 2, however, there is now overlap between packets 1 and 3, forming an interference pattern [Fig. 4(b)]. Nevertheless, the energy of each wave packet can be estimated by arbitrarily defining the wave number $k = 0.105$ nm$^{-1}$ as the border between packets 1 and 3. After application of the wavelet transform [Eq. (7)] to the signal of Fig. 4(a), the wave packets are clearly distinguished [Fig. 4(c)]. A far less severe interference effect is visible between wave packets 1 and 2. Each wave packet is windowed as designated by the dotted lines and the energy is calculated according to Eq. (9). The

TABLE I. Parameters of the wave packets for filtering demonstration. The polarization vector of each basis atom is (0 0 $\sqrt{2}$) and $\zeta$ of each packet is 26.3 nm. Packets are plotted in Fig. 4(a).

| Packet | $A$ (pm) | $k_p$ (nm$^{-1}$) | $z_p$ (nm) | Energy (nm$^3$) |
|---|---|---|---|---|
| 1 | 5.27 | 0.0949 | 135 | $4.58 \times 10^{-4}$ |
| 2 | 4.74 | 0.190 | 169 | $3.71 \times 10^{-4}$ |
| 3 | 5.80 | 0.114 | 405 | $5.54 \times 10^{-4}$ |

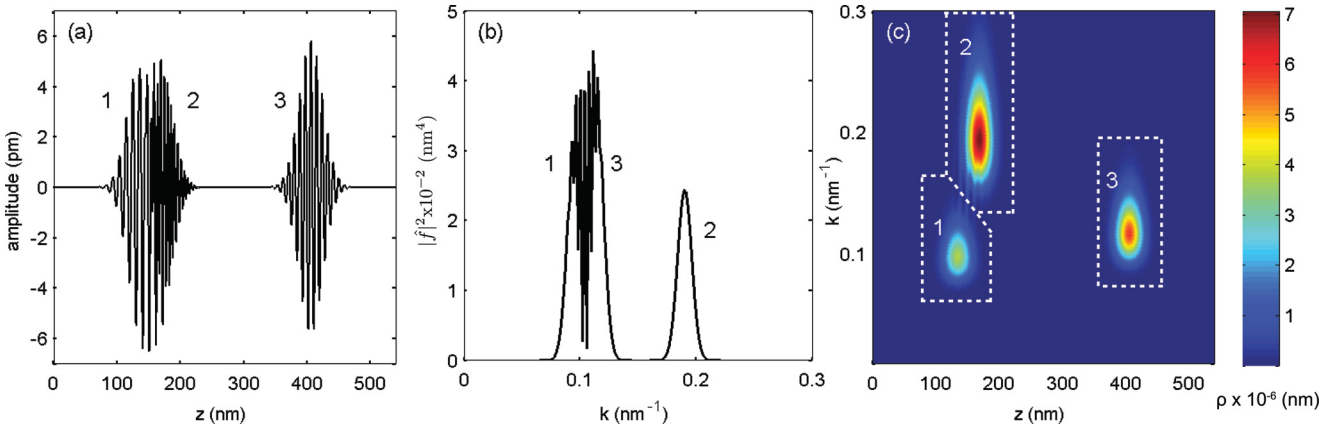


FIG. 4. (Color online) Depiction of enumerated wave packets given by Eq. (21) and Table I for different analytical domains. (a) Wave packets in spatial domain. Packets 1 and 2 interfere spatially. (b) Wave packets in the Fourier domain. Packet 2 has been isolated, but packets 1 and 3 interfere. $k = 0.105$ nm$^{-1}$ is chosen as the arbitrary dividing line. (c) Wave packets in wavelet domain. The abscissa corresponds to Fig. 4(a) and the ordinate corresponds to Fig. 4(b). The wave packets are now separated and individually analyzable. Their energies are summed within the dotted bounds and the results are presented in Table II.

error in the energies calculated in the Fourier and wavelet domains is presented in Table II.

The wavelet transform has reduced the overall error in the calculated energy by two orders of magnitude. The error that yet remains has three contributing factors. First, the interference pattern between packets 1 and 2 creates some error, although it is much less severe than the error introduced by interference in the Fourier domain. Second, the energy in the wavelet domain is computed using a double integral. To achieve levels of accuracy comparable to the integrals in the spatial or Fourier domains, either a higher resolution is required or an integration method more sophisticated than the trapezoidal integration used here is needed. Third, the wavelet energy density continues to decay past the bounding windows depicted here. Making the windows larger mitigates this cutoff error, however, reason demands a limit to the size of a window.

There are a few matters that must be noted about the wavelet transform as depicted in Fig. 4(c). First, the wavelet transform involves three separate quantities with the dimension of length: location, scale, and the atomic displacements. The units of the wavelet energy density [Eq. (10)] $\rho$ are given as nm, which is a simplification of the more cumbersome density expression

$$\frac{\text{nm}^2\ \text{(displacement)} \cdot \text{nm (location)}}{\text{nm (scale)} \cdot \text{nm (location)}}. \tag{22}$$

Second, the surface plot captures aspects of the spatial and Fourier plots. In Fig. 4(c), looking along the $k$ axis is similar to Fig. 4(a) and looking along the $z$ axis is similar to Fig. 4(b). Third, the cross-sectional area and magnitude of packet 2 appear to be larger than the others, whereas the corresponding signal has the smallest amplitude. This apparent inconsistency results from the distortion in $\rho$ when it is plotted against location and wave number instead of location and scale [see Eq. (15) and Sec. II D]. In the $z$-$s$ space, packet 2 has a higher, although sharper, peak than the others, which results in a smaller overall energy. Fourth, although the peaks occur at the same wave numbers as those in the Fourier transform, the distribution is noticeably different. This is the inherent drawback to the wavelet transform: that retaining spatial information in a spectrally sensitive analysis technique increases uncertainty in the wave numbers and vice versa.

Depending on the system, the slight drawback of uncertainty in both location and wave number is more than offset by the additional information obtained. In this case, a group of wave packets, or phonons, were individually distinguished so that their contribution to the total energy could be determined.

TABLE II. Error in computed wave-packet energies by Fourier [Fig. 4(b)] and wavelet transform [Fig. 4(c)] methods compared to the actual energies in Table I.

| Packet | Fourier (%) | Wavelet (%) |
|---|---|---|
| 1 | 6.58 | −0.049 |
| 2 | 0.00 | −0.29 |
| 3 | −5.44 | −0.054 |

### B. Multiple wave-packet simulation

The previous demonstration examined a static system of wave packets. Here, a system of five wave packets is set in motion and the dynamics examined using the wavelet transform. Wave-packet simulation is a popular method for the study of thermal boundary conductance because the frequency-dependent transmission constant can be found on a mode-by-mode basis. Transmissivity is computed for a single packet by comparing the total kinetic and potential energies on either side of the interface before and after the phonon-interface scattering event. Unfortunately, physical energy summation is not possible for simulations studying more complex behavior, such as multiple phonon interactions at an interface or transmission at finite temperature. In these situations, the wavelet transform applied to atomic motion may filter out the extraneous energy and the transmission can

TABLE III. Wave-packet parameters in multiphonon transmission study. Each packet has in common the following parameters: $A = 1.09$ pm and $\zeta = 32.6$ nm.

| Packet | $z_p$ (nm) | $k_p$ (nm$^{-1}$) |
|---|---|---|
| 1 | −114 | −0.460 |
| 2 | −141 | 0.773 |
| 3 | −81.5 | 0.295 |
| 4 | 86.9 | 0.552 |
| 5 | 168 | −0.258 |

be found using wave reflection and transmission equations developed in optics and acoustics:[41]

$$\alpha = 1 - \frac{||A_R||^2}{||A_I||^2} = I\frac{||A_T||^2}{||A_I||^2}, \tag{23}$$

where $I$ is the ratio of acoustic impedances. The quantities $||A_I||^2$, $||A_R||^2$, and $||A_T||^2$ are the energies of the incident, reflected, and transmitted packets, respectively, as calculated by Eq. (9). The first part of Eq. (23) holds for all wave numbers, but the second part of Eq. (23) breaks down upon departure from the small-wave-number limit. Furthermore, the ratio of impedances of the materials may not be known *a priori*. The transmission coefficient will thus be calculated based on the energies of the reflected and incident packets.

A wave-packet simulation was conducted with 5 total packets with parameters defined in Table III. The crystalline system was modeled after the system studied by Schelling *et al.*[18] and is composed of two types of atoms joined at an interface. Atom type A has a mass of 28.09 amu and the mass of atom type B is four times this quantity. The standard Stillinger-Weber potential was used for all atomic interactions.[42] The system measures $2 \times 2 \times 1000$ unit cells and totals 32 000 atoms. A lattice constant of 0.5431 nm was calculated using General Lattice Utilities Program (GULP).[43] The same program was used to find the longitudinal acoustic branch dispersion relation and polarization vector of $(0\,0\,\sqrt{2})$ for both basis atoms. The simulation was carried out using the open source molecular dynamics simulation package LAMMPS.[44] The time step for the simulation was 0.5 fs. Atomic coordinate data was written every 500 steps, corresponding to 0.25 ps.

The 1000 unit cells in the $z$ direction correspond to 2000 $z$ locations because there are two primitive cells per conventional cell in a given direction for fcc silicon. The resulting value for $\Delta z$ is 0.2716 nm. The Brillioun zone edge is located at $k = 1.84$ nm$^{-1}$, however, the stringent value of 0.05 for $\eta$ [Eq. (16)] permits a maximum wave number of only 1.27 nm$^{-1}$. Larger values of $\eta$ increase the risk of aliasing artifacts that can lead to incorrect results and interpretations. Equation (19) can be used because of the periodic boundary conditions in the $z$ direction of the simulation. This results in a minimum wave number of 0.00967 nm$^{-1}$. Between these two limits, 100 points in $k$ space were computed, corresponding to a wave-number resolution of 0.0128 nm$^{-1}$. The spacing of the wavelet filters $\Delta\delta$ was set to 2.7155 nm, which is 10 times more coarse than the spatial sampling $\Delta z$.

The constructed signal and its time evolution are depicted in Fig. 5. The spatial overlap of the packets makes it impossible

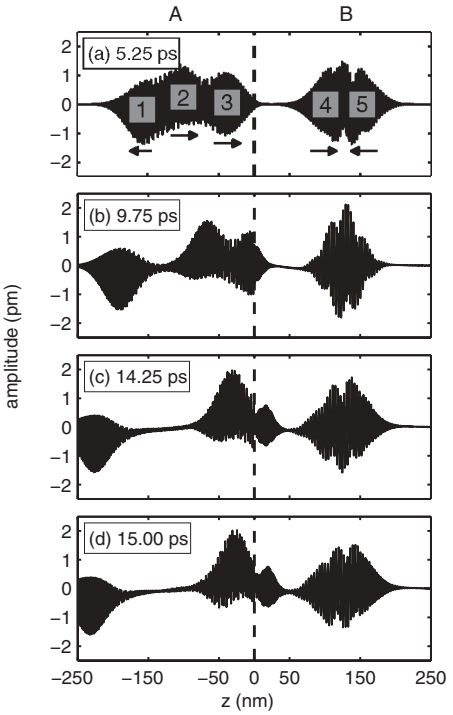


FIG. 5. Longitudinal displacement versus location of a 5 wave-packet system. The domain extends slightly beyond the depicted limits. (a) The packets propagate in the indicated directions. Packet 3 has yet to reach the interface. (b), (c) Packet 3 traverses the interface. (d) Packet 3 has completed its scattering event at the interface. This information on the packet dynamics is obscured by the presence of the other packets.

to discern the motion of individual packets. As in the filtering demonstration, the wavelet transform is able to shed light on the individual packet dynamics (Fig. 6). After release, the packets propagate in the indicated directions. The packet of interest is number 3. Its energy was computed within the dotted windows according to Eq. (9). Using Eq. (23) to calculate the transmission coefficient resulted in a value of 0.89, which is close to the literature value of 0.88.[18] The wave number of the transmitted packet, obtained from the peak of the wavelet energy density, is approximately 0.60 nm$^{-1}$, consistent with the prediction by harmonic lattice dynamics calculations of the dispersion relation. As was the case in Fig. 4(c), interference effects manifest themselves as ridges between packets 1 and 2, and to a lesser extent, packets 4 and 5.

The ability to calculate the transmission coefficient in wavelet space was further validated by a series of simulations where a single wave packet was scattered at the interface. The wave-packet wave numbers ranged from 0.092 to 1.10 nm$^{-1}$ and each wave packet originated in material A, 550 unit cells from the A/B interface. The domain was identical to that of Fig. 6 except the interface was located at $z = 135.8$ nm. In analyzing the incident and reflected wave packets, the $\eta$ parameter [Eq. (16)] was set to 1 in order to allow for complete windowing of the wave packets. Such a high $\eta$ parameter is justified by the pristine system with only one explicitly defined mode which prevents aliasing artifacts. The results are depicted in Fig. 7 and show excellent agreement with the literature values for longitudinal acoustic mode transmission.[18]

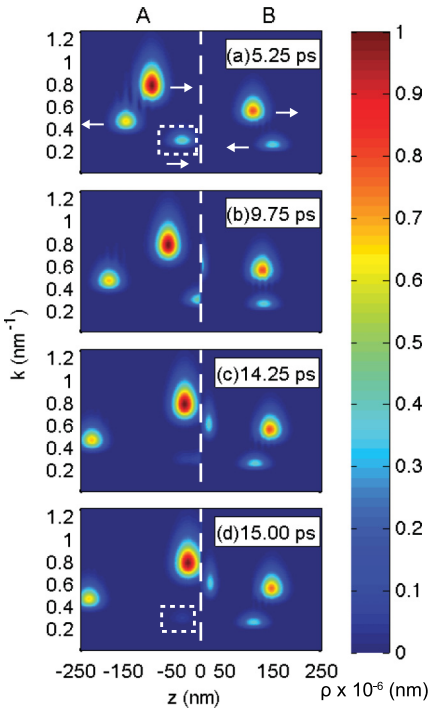


FIG. 6. (Color online) The wavelet transform of Fig. 5. Individual packet features are resolved. Packet 3 is windowed and its incident and reflected energies are calculated in (a) and (d), respectively. The peak wave number of packet 3 before and after scattering is noted and compared to predictions from lattice dynamics.

The interfaces studied here are of the least complexity in order to provide comparison to analytical and published predictions. As a result, the wave-packet transmission process is orderly. At more complex interfaces, it is likely that some of the packet energy would leak into packet states of different polarizations, branches, and even directions. This type of mode conversion would be detectable using multiple wavelet transforms of the same system that focus on a particular branch and polarization.

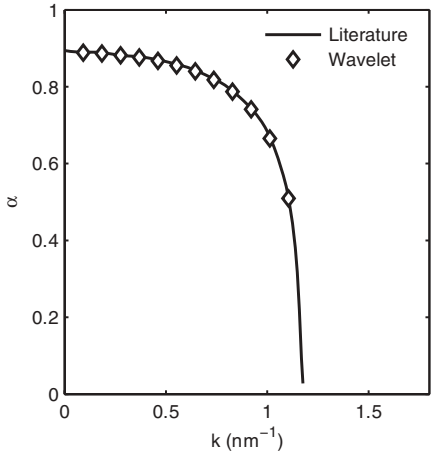


FIG. 7. Wave-packet transmission as a function of wave number as measured by the wavelet transform. Beyond the maximum wave-packet wave number of 1.10 nm$^{-1}$, uncertainty in the wavelet transform generates modes that abut against the Brillioun zone edge, interfering with the calculations. The reference line is a spline fit of the frequency-dependent data from Ref. 18 that was converted to wave-number space through the Si dispersion calculated by GULP.

TABLE IV. Wave-packet energy over time and its distribution among $k_p$, $2k_p$, and $>2k_p$ modes. The total energy decreases as energy scatters into modes lower than $k_p$.

| Time (ps) | Energy (nm$^3$) | $k_p$(%) | $2k_p$(%) | $>2k_p$(%) |
|---|---|---|---|---|
| 0.00 | 869.6 | 99.8 | 0.2 | 0.0 |
| 4.00 | 602.3 | 95.0 | 3.4 | 1.6 |
| 8.75 | 215.6 | 86.3 | 4.4 | 9.3 |
| 20.00 | 120.4 | 47.0 | 6.6 | 46.4 |

### C. Anharmonic wave-packet simulation

The wave packets of the previous demonstrations were perturbations to an otherwise ideal, zero Kelvin system. Here, a wave packet is studied whose higher amplitude is more representative of the displacements that might be found in a finite-temperature system. The domain has the same dimensions as that of the previous section and is entirely made up of material A. One wave packet was introduced into the system with the following parameters: $k_p = 0.092$ nm$^{-1}$,

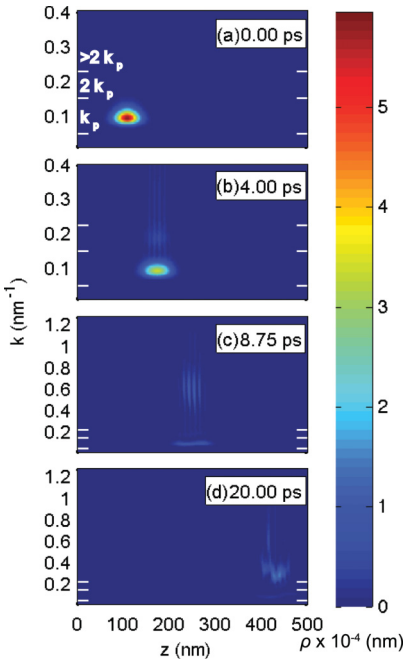


FIG. 8. (Color online) Anharmonic breakdown of a wave packet viewed using the wavelet transform. Hash marks delineate regions of energy summation (Table IV). (a) The wave packet is generated with a peak wave number $k_p$ of 0.092 nm$^{-1}$. (b) Anharmonic interaction redistributes energy into the $2k_p$ region, representing a three-phonon annihilation scattering process. (c) Energy is further partitioned into the 0.60-nm$^{-1}$ region; $2k_p$ modes are still present. Note the change in ordinate scale. (d) The $2k_p$ mode has largely disappeared. The high-wave-number modes have diffused into a less coherent structure.

$\zeta = 32.6$ nm, and $A = 65.2$ pm where the amplitude is about a factor of 60 larger than in the previous section.

Much of the initial energy is converted to an induced strain field due to the Grüneisen theory of thermal expansion (Table IV).[45] This energy is not visible in the wavelet transform because of the restrictions on the allowed wave number, i.e., the induced strain field is nearly zone center with a wave number lower than 0.00967 $nm^{-1}$. The original mode propagates and some of the energy scatters into the $2k_p$ and higher modes [Fig. 8(b) and Table IV]. The wave numbers are sufficiently small such that the Debye approximation is valid, thus the energy scattering into the $2k_p$ mode represents a three-phonon annihilation scattering process. The fraction of energy in the $k_p$ mode diminishes while the energy content of the $2k_p$ and higher modes grows [Figs. 8(c) and 8(d)]. The wavelet transform particularly elucidates changes in the modal energy distributions of the original wave packet as well as the higher-wave-number modes. The original wave packet undergoes a "flattening" and "shearing" process after about 4 ps [Figs. 8(b) and 8(c)]. This can not be explained by dispersive effects since modes in this range of wave numbers behave Debye-like. Also, after 8.75 ps, the energy distribution of the higher-wave-number modes transitions from an orderly arrangement of mutually interfering modes to a less coherent structure, accompanied by a decrease in mean wave number from 0.44 to 0.28 $nm^{-1}$ [Figs. 8(c) and 8(d)]. By 20 ps, the energy in the $2k_p$ mode has become mixed with the higher modes. Studying these types of transitions with the wavelet transform may provide insight into phonon dynamics beyond the harmonic approximation.

## IV. SUMMARY

In summary, the wavelet transform was presented and applied to the analysis of phonon transport problems in molecular dynamics simulation. The wavelet transform itself is a tool akin to the Fourier transform. It not only decomposes a signal into its spectral components, but also retains the spatial location where each vibration occurred. The discretization of the continuous wavelet transform was treated with attention to practical implementation. Three applications were explored. In the filtering demonstration, the wavelet transform calculated the correct energies of the interfering wave packets when spatial and Fourier methods failed. In the second application, the wavelet transform technique quantitatively reproduced the expected results of interface scattering. In the wavelet domain, the packet scattered into the correct wave number and with the correct transmissivity. Finally, the wavelet transform was used to observe a high-amplitude wave packet and elucidate the complexity of the scattering process with respect to space and wave number. The nanometer-resolved wave-number information that the wavelet transform provides has thus been validated so that the technique may be used to investigate more sophisticated systems in nanoscale thermal transport.

## ACKNOWLEDGMENTS

The authors would like to acknowledge financial support from the Air Force Office of Scientific Research (Grant No. FA9550-09-1-0245), as well as N. Q. Le, T. S. English, J. C. Duda, and A. J. H. McGaughey for their insightful discussion.

*chb2fd@virginia.edu
†pamela@virginia.edu

[1] L. D. Hicks and M. S. Dresselhaus, Phys. Rev. B **47**, 12727 (1993).
[2] L. E. Bell, Science **321**, 1457 (2008).
[3] C. J. Vineis, A. Shakouri, A. Majumdar, and M. G. Kanatzidis, Adv. Mater. **22**, 3970 (2010).
[4] P. Pichanusakorn and P. Bandaru, Mater. Sci. Eng., R **67**, 19 (2010).
[5] A. Shakouri, Annu. Rev. Mater. Res. **41**, 399 (2011).
[6] K. W. J. Barnham and G. Duggan, J. Appl. Phys. **67**, 3490 (1990).
[7] G. Chen, *Nanoscale Energy Transport and Conversion* (Oxford University Press, Oxford, UK, 2005).
[8] W. A. Little, Can. J. Phys. **37**, 334 (1959).
[9] E. T. Swartz and R. O. Pohl, Rev. Mod. Phys. **61**, 605 (1989).
[10] M. T. Dove, *Introduction to Lattice Dynamics* (Cambridge University Press, Cambridge, UK, 1993).
[11] A. Ward and D. A. Broido, Phys. Rev. B **81**, 085205 (2010).
[12] V. Narayanamurti, H. L. Störmer, M. A. Chin, A. C. Gossard, and W. Wiegmann, Phys. Rev. Lett. **43**, 2012 (1979).
[13] T. S. English, J. C. Duda, J. L. Smoyer, D. A. Jordan, P. M. Norris, and L. V. Zhigilei, Phys. Rev. B **85**, 035438 (2012).
[14] N. Mingo and L. Yang, Phys. Rev. B **68**, 245406 (2003); **70**, 249901(E) (2004).
[15] J.-S. Wang, J. Wang, and N. Zeng, Phys. Rev. B **74**, 033408 (2006).
[16] D. A. Young and H. J. Maris, Phys. Rev. B **40**, 3685 (1989).
[17] H. Zhao and J. B. Freund, J. Appl. Phys. **97**, 024903 (2005); **97**, 109901(E) (2005).
[18] P. K. Schelling, S. R. Phillpot, and P. Keblinski, Appl. Phys. Lett. **80**, 2484 (2002).
[19] L. Sun and J. Y. Murthy, J. Heat Transfer **132**, 102403 (2010).
[20] M. Hu, P. Keblinski, J.-S. Wang, and N. Raravikar, J. Appl. Phys. **104**, 083503 (2008).
[21] L. Hu, L. Zhang, M. Hu, J.-S. Wang, B. Li, and P. Keblinski, Phys. Rev. B **81**, 235427 (2010).
[22] N. A. Roberts and D. G. Walker, J. Appl. Phys. **108**, 123515 (2010).
[23] Z. T. Tian, B. E. White, Jr., and Y. Sun, Appl. Phys. Lett. **96**, 263113 (2010).
[24] C. Kimmer, S. Aubry, A. Skye, and P. K. Schelling, Phys. Rev. B **75**, 144105 (2007).
[25] A. J. H. McGaughey and M. Kaviany, Phys. Rev. B **69**, 094303 (2004); **79**, 189901(E) (2009).
[26] J. E. Turney, E. S. Landry, A. J. H. McGaughey, and C. H. Amon, Phys. Rev. B **79**, 064301 (2009).
[27] J. M. Dickey and A. Paskin, Phys. Rev. **188**, 1407 (1969).
[28] C. Kittel, *Introduction to Solid State Physics* (Wiley, New York, 2004).
[29] To be sure, the issue of locality is addressed by the short-time or windowed Fourier transform which is a modification of the Fourier transform. The focus shall remain on the wavelet transform and its contrast to the Fourier transform because (1) the Fourier transform

is vastly more familiar to the nanoscale community as it is the basis of some of its most important concepts, including density of states, and (2) the wavelet transform contains additional advantages over the short-time Fourier transform. Interested readers are directed to Kaiser for a more in-depth comparison of the two techniques (Ref. 36).

[30]M. Farge, Annu. Rev. Fluid Mech. **24**, 395 (1992).

[31]P. Goupillaud, A. Grossman, and J. Morlet, Geoexploration **23**, 85 (1984).

[32]S. Mallat, IEEE Trans. Pattern Anal. Mach. Intell. **11**, 674 (1989).

[33]M. Antonini, M. Barlaud, P. Mathieu, and I. Daubechies, IEEE Trans. Image Process. **1**, 205 (1992).

[34]C. Torrence and G. P. Compo, Bull. Am. Meteorol. Soc. **79**, 61 (1998).

[35]J. Shiomi and S. Maruyama, Phys. Rev. B **73**, 205420 (2006).

[36]G. Kaiser, *A Friendly Guide to Wavelets* (Birkhauser, Boston, 1994).

[37]M. Plancheral and M. Leffler, Rend. Circolo Mat. (Palermo) **30**, 289 (1910); E. C. Titchmarsh, Proc. London Math. Soc. **23**, 279 (1925).

[38]R. N. Bracewell, *The Fourier Transform and its Applications* (McGraw-Hill, New York, 1999).

[39]D. Jordan, R. W. Miksad, and E. J. Powers, Rev. Sci. Instrum. **68**, 1484 (1997).

[40]This result can be derived from Eqs. (13) and (15).

[41]M. Born and E. Wolf, *Principles of Optics* (Pergamon, New York, 1980).

[42]F. H. Stillinger and T. A. Weber, Phys. Rev. B **31**, 5262 (1985); **33**, 1451(E) (1986).

[43]J. D. Gale and A. L. Rohl, Mol. Simul. **29**, 291 (2003).

[44]S. Plimpton, J. Comput. Phys. **117**, 1 (1995).

[45]S. Sinha, P. K. Schelling, S. R. Phillpot, and K. E. Goodson, J. Appl. Phys. **97**, 023702 (2005).